Biochimica et Biophysica Acta 1840 (2014) 3170–3180

Contents lists available at ScienceDirect

Biochimica et Biophysica Acta

journal homepage: www.elsevier.com/locate/bbagen

Anti-interleukin-6 receptor antibody (MR16-1) promotes muscle regeneration via modulation of gene expressions in infiltrated macrophages

Ryo Fujita [a], Fumimori Kawano [a], Takashi Ohira [b], Naoya Nakai [a], Tsubasa Shibaguchi [b], Norihiro Nishimoto [c], Yoshinobu Ohira [a,b,*]

[a] Graduate School of Medicine, Osaka University, Japan
[b] Graduate School of Frontier Bioscience, Osaka University, Japan
[c] Laboratory of Immune Regulation, Wakayama Medical University, Japan

ARTICLE INFO

Article history:
Received 25 August 2013
Received in revised form 6 January 2014
Accepted 8 January 2014
Available online 15 January 2014

Keywords:
Muscle regeneration
Muscle injury
Anti-mouse IL-6 receptor (IL-6R) antibody
Fibrosis

ABSTRACT

Background: Although rat anti-mouse IL-6 receptor (IL-6R) antibody (MR16-1) has been reported to effectively ameliorate various tissue damages, its effect on skeletal muscle regeneration has not been determined. Moreover, the localization, persistence and duration of action of this reagent in damaged tissues after systemic administration have not been assessed.
Methods: The MR16-1 was administered i.p. immediately after cardiotoxin (CTX)-induced muscle damage on mice.
Results: MR16-1 administered i.p. was observed only to the damaged muscle. This delivered MR16-1 was dramatically decreased from 3 to 7 days post-injury concomitantly with a reduction of IL-6R expression. This reduction of the MR16-1 level in the damaged muscle was not rescued by additional administration of MR16-1, suggesting the short half-life of MR16-1 was not the factor for the remaining levels. In addition, a significant inhibitory effect of MR16-1 on phosphorylation of the signal transducer and activator of transcription 3 was observed in the macrophage-enriched area of damaged muscle 3 days after injury. Finally, the acceleration of muscle regeneration observed at day 7 post-injury following MR16-1 treatment was associated with reduced expression of fibrosis-related genes, such as interleukin-10 and arginase, in the infiltrated macrophages.
Conclusions: These results suggest that MR16-1 which was found primarily localized in infiltrated macrophages in the damaged muscle might facilitate muscle regeneration via immune modulation.
General significance: These findings are deemed to provide further insight into the understanding not only of MR16-1 treatment on muscle regeneration, but also of the other anti-cytokine treatment on the cytokine-related disease.

1. Introduction

Regeneration of skeletal muscle following injury is a coordinated process that involves proliferation and differentiation of muscle stem cells called satellite cells, leading to new fiber formation [1,2]. The first step of regeneration is the inflammation phase. This is a highly complex process that requires infiltration of inflammatory cells; the release of growth factors and pro- or anti-inflammatory cytokines; and is closely linked to myogenesis [3,4]. Well-regulated inflammation after injury is critical for myogenesis. Lack of a successful inflammatory response, which is often associated with incomplete muscle tissue reconstruction, such as in severe fibrosis, results in poor muscle regeneration [5,6].

Neutrophils, followed by macrophages, rapidly infiltrate into damaged muscle at the start of muscle inflammation [7]. Although infiltration of neutrophils is generally considered to have an adverse influence on muscle regeneration [8], macrophages have apparently conflicting roles, which may be partly explained by the existence of a phenotypically distinct population that can promote muscle injury and repair [9–12]. Heterogeneity of macrophages has recently been recognized as a result of adaptation from a pro-inflammatory to an anti-inflammatory phenotype in particular micro-environments, and vice versa [13–15]. This phenotypical change of macrophages has a strong modulatory effect on gene expression profiles in cells, such as cytokines, that is essential for maintaining a balance between inflammation and acceleration of myogenesis [9,16].

Abbreviations: MR16-1, rat anti-mouse IL-6 receptor antibody; CTX, cardiotoxin; STAT3, signal transducer and activator of transcription 3; LMD, laser capture microdissection

* Corresponding author at: Graduate School of Medicine, Osaka University, Health and Sport Science Research Building, 1-17 Machikaneyama-cho, Toyonaka City, Osaka 560-0043, Japan. Tel.: +81 6 6850 6018.
E-mail address: oyoshinobu@gmail.com (Y. Ohira).

0304-4165/$ – see front matter © 2014 Elsevier B.V. All rights reserved.
http://dx.doi.org/10.1016/j.bbagen.2014.01.014

Both positive and negative participation of pro-inflammatory cytokines, including tumor necrosis factor-α (TNF-α) [17,18], interferon-γ [19], and interleukin-6 (IL-6) [20–23], has been reported in the muscle regeneration processes. TNF-α, which is secreted by a wide range of inflammatory cells and by damaged muscle, is considered to be a pathological factor in muscle regeneration from the standpoint that it inhibits Notch 1 expression [24] and insulin-like growth factor-1 signaling [25]. Moreover, Grounds and Torrisi reported that inhibition of TNF-α signaling through the use of an anti-TNF-α drug caused greater reduction and delayed breakdown of myofibers following necrosis in *mdx* mice [26]. On the other hand, anti-TNF-α drugs should be used with caution, because there are reports suggesting that TNF-α is required for muscle regeneration through p38 activation [17,18].

In addition, IL-6, another major pro-inflammatory cytokine, is also known to have bimodal functions. By general consensus, IL-6 is recognized to have roles in immune responses and inflammation, such as antibody production through B cell maturation and macrophage differentiation [27,28]. Furthermore, escalating evidence indicates that excess IL-6 is linked to various pathological conditions, including rheumatoid arthritis (RA) and spinal cord injury [29–31]. Human clinical trial was conducted to treat RA by a specific humanized neutralizing antibody against IL-6R (MRA) with promising effects [30].

In skeletal muscle, studies using mice that over-express IL-6 have suggested that several proteolytic systems, such as the cathepsin B-mediated lysosomal pathway, the cathepsin B + L mediated lysosomal pathway and the ubiquitin–proteasome pathway, were significantly activated in the presence of a high concentration of IL-6. But all of these changes were inhibited by treatment with an anti-mouse IL-6 receptor antibody (MR16-1) [22]. That MR16-1 binds specifically mouse IL-6R and blocks transmitting of IL-6 signals, but does not cross-react human IL-6R [32,33]. Further, it has been reported that IL-6 plays a critical role in satellite cell-mediated hypertrophic growth [21,34], suggesting that the inhibition of IL-6 signaling by MR16-1 has adverse effects on muscle regeneration. In other words, the role(s) of MR16-1 in the plasticity of skeletal muscle is not well understood. Furthermore, although MR16-1 treatment has gained popularity for the treatment of a variety of diseases, little work has been done to elucidate the mechanisms underlying the efficacy of MR16-1 in these contexts, including clarification of the localization, persistence and duration of activity of MR16-1. Therefore, the assessment of the effects of MR16-1 in various models and clarification of the mechanisms of this agent would be useful information for the treatment of not only muscle injury but also other human diseases.

The present study was performed to evaluate the therapeutic potential of MR16-1 in the regeneration of injured skeletal muscle.

2. Materials and methods

2.1. Animals

This study was approved by the Animal Use Committee at Osaka University and was performed following the Japanese and American Physiological Society's Guide for the Care and Use of Laboratory Animals. Eight-week-old male C57BL/6J mice (CLEA Japan, Tokyo, Japan) and 8- to 9-week-old male IL-6 knock-out (IL-$6^{-/-}$) mice were used. The IL-$6^{-/-}$ mice had a C57BL/6J background. Each mouse was housed in a cage (20 × 10 cm with 10-cm height). Solid food (CE-2; CLEA Japan) and water were supplied ad libitum. Temperature and humidity in the animal room were maintained at ~23 °C and ~55% under a 12:12 h light:dark cycle.

2.2. Muscle injury and MR16-1 treatment

To induce muscle injury, cardiotoxin (CTX) (*Naja mossambica mossambica* venom; Sigma, St. Louis, MO) was used. Briefly, mice were anesthetized by i.p. injection of pentobarbital sodium (5 mg/100 g body weight). The hairs of the left leg were shaved and the tibialis anterior (TA) muscle was exposed by incision of the skin (~5 mm). Five μl of CTX (0.03%) was injected into the medial and lateral regions of the TA muscle using a microsyringe (Hamilton 701N; Hamilton Co., Reno, NV). The skin was then sutured and isodine was applied to the surgical site to avoid infection. The contralateral TA muscle served as the sham-operated control without CXT injection (CON).

The mice were randomly assigned to 2 groups, a group with (CTX + MR16-1, n = 18) and one without (CTX, n = 30) i.p. administration of MR16-1 (2 mg/mouse) immediately after CTX injection. Mice of the former group were administered MR-16-1 either once (immediately after CTX injury; n = 12) or twice (immediately and 3 days after CTX injury; n = 6). IL-$6^{-/-}$ mice were also treated with CTX in the same way explained above (n = 16). Mice in each group were randomly euthanized at either 3 (CTX, n = 15; CTX + MR16-1, n = 6; IL-$6^{-/-}$, n = 10) or 7 (CTX, n = 15; CTX + MR16-1, n = 6; IL-$6^{-/-}$, n = 6) days after the CTX injection under anesthesia with pentobarbital sodium (5 mg/100 g body weight). The TA muscles were sampled bilaterally, and the excess fat and connective tissues were removed and quickly weighed. The muscles were stretched at an optimum length in vivo on a cork and pinned, frozen in isopentane cooled with liquid nitrogen, and stored at −80 °C until analyses.

2.3. Histological and immunohistochemical analyses

Cross sections (10-μm thickness) of the midbelly region of muscle were cut in a cryostat (−20 °C) for immunohistochemical analysis of the morphological properties. Hematoxylin and eosin (H&E) staining was carried out to check the degree of damage and the regeneration process in the left TA. Briefly, cross sections were air-dried at room temperature and fixed in 10% formalin (Nacalai Tesque, Kyoto, Japan) for 10 min. Then, the cross sections were stained with Mayer's hematoxylin (Wako, Osaka, Japan) and 0.5% eosin (Merck, Rahway, NJ).

The cross sections were initially fixed in 4% (wt/vol) paraformaldehyde in 0.1 M phosphate buffer (pH 7.4) for 15 min and processed for immunohistochemical analyses [35]. Mouse Ig blocking reagent and a Vector M.O.M. immunodetection kit (Vector Laboratories, Burlingame, CA) were applied to prevent the non-specific binding of a secondary anti-mouse antibody on the endogenous mouse tissue Igs in the cross sections labeled with mouse monoclonal primary antibody. The cross sections were incubated at 4 °C overnight with primary antibodies as follows: rat monoclonal anti-CD68 (1:200; Abcam, Cambridge, MA), rat monoclonal anti-neutrophil marker (1:100; Santa Cruz Biotechnology, Santa Cruz, CA), rat monoclonal anti-CD11b (1:200; Abcam), rabbit polyclonal anti-dystrophin (1:200; Thermo Scientific, Rockford, IL), rabbit polyclonal anti-desmin (1:200; Thermo Scientific), rabbit polyclonal anti-IL-6R (1:200; Santa Cruz Biotechnology), mouse monoclonal anti-myogenin (1:200; ABM, Vancouver, Canada) and neonatal myosin heavy chain (nMyHC) (1:200; Leica Biosystems, Newcastle, UK). M.O.M. biotinylated anti-mouse IgG (Vector Laboratories) secondary antibody was used following the application of mouse monoclonal primary antibody. Lastly, the cross sections were washed with 0.1 M phosphate buffered saline (PBS) and mounted with VECTASHIELD containing 4′,6-diamidino-2-phenylindole (DAPI) (Vector Laboratories) for nuclear staining. Immunoreactions without primary antibodies were also performed to evaluate the specificity of staining. The cells that were stained for desmin, myogenin, and nuclei were counted twice in three damaged regions within the square shown in Fig. 1 (n = 6/group). The nMyHC positive areas in three damaged regions (100 to 400 myotubes) per mouse were determined by NIH ImageJ software (n = 3–4/group). The two serial sections per mouse were measured in each analysis. Stained cross sections were visualized using a fluorescent microscope (BX50; Olympus, Tokyo, Japan), and the images were arranged using Adobe Photoshop software.

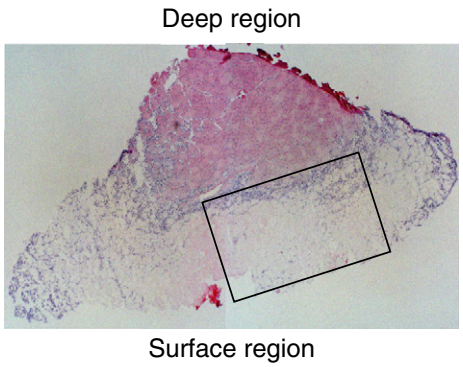

Fig. 1. Cross-section of the tibialis anterior muscle stained with hematoxylin and eosin, 3 days after induction of damage by injection of cardiotoxin. The area within the square was used for histological analyses.

2.4. ELISA for IL-6

IL-6 levels in muscles were determined using a commercially available sandwich ELISA kit (RayBio Inc., Norcross, GA) following the manufacturer's instructions. The whole TA muscles (up to 60 mg) were homogenized in 500 μl ice-cold PBS. The muscle homogenates were then centrifuged at 15,000 rpm for 15 min at 4 °C. The supernatant (3 mg/ml) diluted 1:5 sample diluent buffer was used for ELISA. The protein concentration of each sample was measured using the DC protein assay kit (Bio-Rad Laboratories, Hercules, CA) standardized to BSA according to the manufacturer's protocol.

2.5. Proximity ligation assay

For the proximity ligation assay (PLA), cross sections (10 μm thickness) were cut in a cryostat and mounted on a superfrost microslide glass with an aminopropylsilane coating. Pre-treatments of samples for PLA reactions were almost identical to the procedure described above for the immunohistochemical analyses, except for the blocking reagent and the processes after incubation of primary antibodies. Duolink blocking reagent was applied to the sections, and then the sections were incubated in a pre-heated humidity chamber for 30 min at 37 °C before overnight incubation of primary antibodies at 4 °C. The primary antibodies used for the detection of IL-6 receptor (IL-6R) and phosphorylated signal transducer and activation of transcription 3 (pSTAT3) were rabbit IL-6R (1:200; Santa Cruz Biotechnology) and rabbit p-STAT3 (Tyr705) (1:100; Cell Signaling Technology, Beverly, MA), respectively. After washing of the cross sections with Duolink wash buffer (Tris buffered saline with Tween 20), incubation with anti-rabbit IgG PLA probes and analysis with a Duolink detection kit 613 (Olink) were conducted following the manufacturer's protocol with some modifications. The hybridization and ligation times were extended to 30 min and the concentration of Duolink polymerase was increased 1.5-times vs. the manufacturer's recommendation. Nuclei were stained with the Hoechst 33342 included in the detection solution. For the detection of administered MR16-1, cross sections were reacted with anti-rat IgG PLA probes without incubation with any primary antibodies.

Staining was verified using the appropriate negative and positive controls to ensure the specificity of staining. As a positive control for the detection of IL-6R and intraperitoneally administered MR16-1, the cross sections of damaged muscles without MR16-1 administration were incubated with MR16-1 overnight at 4 °C, followed by the standard processes of PLA (Fig. S1). As a negative control for IL-6R and pSTAT3 staining, the cross sections were prepared without primary antibodies following the standard processes as described above (Fig. S2). Stained cross sections were visualized using a fluorescent microscope (BX50; Olympus), and the images were arranged using Adobe Photoshop software. PLA signals were counted by a Duolink Image Tool (Olink Biosciences, Uppsala, Sweden). The number of PLA signals was counted in the areas with infiltration of mononucleated cells and swollen necrotic fibers. PLA signals per 10,000 μm^2 were then calculated.

2.6. Western blot analysis

Tissue samples were homogenized in lysis buffer (20 mM Tris–HCl with pH 7.6, 150 mM NaCl, 50 mM NaF, 1 mM Na_3VO_4, and 1% Triton X-100) with a protease inhibitor cocktail (Millipore, Bedford, MA) using a hand-held homogenizer. The homogenates were stirred by rotation of tubes overnight at 4 °C, and then centrifuged at 15,000 rpm for 10 min at 4 °C. The supernatant, collected as a detergent-soluble fraction, was stored immediately at −80 °C for subsequent use in western blot analyses. The protein concentration was determined using a NanoOrange Protein Quantitation kit (Molecular Probes, Eugene, OR) following the manufacturer's protocol.

Equal amounts of protein (1.5 μg/μl) were denatured in sample buffer (5 min, 99 °C) and separated on 10% SDS-PAGE gels. Separated proteins were transferred onto polyvinylidene difluoride membranes and blocked in 5% (wt/vol) skim milk diluted in Tris-buffered saline with 0.1% (vol/vol) Tween 20 (TBST) or Blocking-one P (Nacalai Tesque) for 1 h at room temperature. Following the blocking, primary antibodies against pSTAT3 (Tyr705), STAT3 (Cell Signaling Technology) and IL-6R (Santa Cruz Biotechnology) diluted in 5% (wt/vol) bovine serum albumin in TBST were applied, and the membranes were incubated at 4 °C overnight. The membranes were then washed with TBST and incubated for 1 h at room temperature with secondary anti-rabbit IgG horseradish peroxidase (HRP)-conjugated antibodies (Cell Signaling Technology). Following the detection of specific antibodies, the same membranes were stripped with WB stripping solution (Nacalai Tesque) for 2 h at room temperature and reprobed with rabbit anti-Pan-actin antibody (Cell Signaling Technology) to confirm that equal amounts of proteins were loaded. Detection of intraperitoneally administered MR16-1 in the muscle was performed using an anti-rat IgG HRP-conjugated antibody without any primary antibodies, because MR16-1 was derived from rat IgG. MR16-1 itself (10 ng), dissolved in the sample buffer, was electrophoresed as a positive control to identify the band for rat IgG. All bands were visualized by ECL-plus (GE Healthcare, Buckinghamshire, UK) with an ECL mini camera (GE Healthcare). The band density was analyzed by NIH ImageJ software.

2.7. Conventional RT-PCR and real-time PCR

Total RNA was extracted from TA muscle using ISOGEN (Nippon Gene, Toyama, Japan) according to the manufacturer's instruction. Total RNA (1 μg) was reverse-transcribed using a Super-Script™ II Reverse Transcriptase kit (Invitrogen, Carlsbad, CA) with Oligo dT primers. Then, 2 μl of the first-strand RT product was amplified using an Expand High Fidelity PCR System (Roche, Mannheim, Germany) with specific primers for glyceraldehyde 3-phosphate dehydrogenase (GAPDH) (185 bp), IL-6R (615 bp), and gp130 (687 bp). The PCR primers for conventional RT-PCR were as follows: GAPDH, sense 5′-ACTCCCACTCTTCC ACCTTC-3′ and antisense 5′-TCTTGCTCAGTGTCCTTGC-3′; 18S rRNA, sense 5′-TCAAGAACGAAAGTCGGAGGTT-3′ and antisense 5′-GGACAT CTAAGGGCATCACAG; IL-6R, sense 5′-TGTCAACGCCATCTGTGAGTGG-3′ and antisense 5′-ACTTTCGTACTGATCCTCGTGG-3′; and gp130, sense 5′-CCGCGTACACAGATGAAGGTGGGAAAGA-3′ and antisense 5′-GCTG ACTGCAGTTCTGCTTGA-3′ (purchased from Invitrogen). Ten μl of amplification product was subjected to electrophoresis on 4% agarose gel containing ethidium bromide for visualization. In the case of real-time PCR analysis, a High Capacity RNA-to-cDNA kit (Applied Biosystems, Foster City, CA) was used to obtain cDNA. Real-time PCR was performed using commercially designed Taqman gene expression assays {specific for IL-6R, IL-6, TNF-α, interleukin-1β (IL-1β), inducible nitric oxide

(iNOS), interleukin-10 (IL-10), arginase, and GAPDH} and Taqman Universal PCR master mix (Applied Biosystems). The quantitative data were obtained in duplicate on a 384-well plate using an ABI Prism 7900 HT Sequence Detection System (Applied Biosystems). Primer pairs were designed at intron/exon boundaries to avoid genomic DNA contamination. The threshold cycle was calculated by SDS software (version 2.3; Applied Biosystems).

All data were obtained using the standard curve method and normalized by GAPDH level (internal control). Data were expressed as the fold increase versus the control value.

2.8. Laser capture microdissection system and real-time RT-PCR

Cross sections (20-μm thickness) were cut in a cryostat and mounted on foil-coated slide glass (90 FOIL-SL25; Leica Microsystems, Heidelberg, Germany). The cross sections were fixed in 70% cold ethanol for 3 min, briefly rinsed in diethyl pyrocarbonate (DEPC)-treated cold water, stained with toluidine blue (pH 7.0) for 2 min, and then rinsed two times in DEPC-treated cold water and dried completely. Isolation of the macrophage-enriched region with infiltrated mononuclear cells (macrophages) was performed using a laser capture microdissection (LMD) system (Leica Microsystems). The isolated regions were collected into a PCR tube containing 30 μl of ISOGEN (Nippon Gene). Total RNA was extracted from 12 muscle sections (equivalent to 10 mm^2/sample) and 5 μl of RNA solution was reverse-transcribed using a High Capacity RNA-to-cDNA kit (Applied Biosystems) according to the manufacturer's instructions, followed by real-time PCR using the protocols described above. Total RNA extracted from the contralateral muscle cross sections (equivalent to 10mm mm^2/sample) was used as the control. All data were normalized against GAPDH (internal control).

2.9. Statistical analysis

Values were expressed as the means ± SEMs. Statistical analyses were performed by ANOVA, followed by Scheffé's post-hoc test, and Student's *t*-test using SPSS ver. 10.0 (SPSS Japan Inc., Tokyo, Japan) when appropriate. Statistical significance was accepted at $p < 0.05$.

3. Results

3.1. Body weight and muscle wet weight

Intramuscular CTX injection and i.p. MR16-1 administration had no effect on the body weight at any time points (Table S1). The intact TA wet weight relative to body weight remained unchanged during the experimental period. Three days after CTX injection, the TA weights were the same in all groups. However, the relative wet weights in the damaged muscles (2.13 ± 0.03) were significantly less than those in the contralateral controls (1.58 ± 0.05) at 7 days after CTX injection (25.44 ± 2.49% reduction, $p < 0.001$). Furthermore, the relative TA wet weights at the 7th day after CTX injection were also significantly less than those of the injured muscles at day 3 (1.92 ± 0.05) (17.91 ± 2.74% reduction, $p < 0.005$). Significant differences were not seen between the damaged muscles with and those without treatment of MR16-1 at any time points.

3.2. Morphological changes of muscle after CTX injection

Histological examination was also performed in the cross sections of muscle to confirm the damage at day 3 post-injury (Fig. 1). Changes of muscle morphology were clearly evident, especially with respect to the surface area. The characteristics of necrotic fibers generally consisted of round-shaped cytoplasma that were lightly stained by eosin, and no peripheral nuclei. However, fibers in the deep region were intact. Note that the damaged areas were invaded by inflammatory cells. These patterns caused by CTX injection agreed with other reports [36,37]. The surface area, indicated by the square, was utilized for immunohistochemical analyses of myogenin, desmin and nMyHC.

3.3. Delivery of MR16-1 to the damaged regions

The localization of rat IgG in TA muscle was analyzed to check the delivery of administered MR16-1 at 3 days after the induction of injury. Bands for the heavy chain (HC) and light chain (LC) of rat IgG were noted following western blot analyses in the damaged muscle treated with MR16-1 (Fig. 2A). However, these bands were not observed in the contralateral intact muscle even with MR16-1 treatment. The localization of MR16-1 in this specific muscle region was further checked by PLA. PLA signals were hardly detectable in the cross sections of either the undamaged or damaged muscles without MR16-1 treatment (Fig. 2B a and c). The PLA signals were predominately detected in the damaged area with necrotic fibers characterized by circular shape, disappearance of peripheral nuclei, and infiltrated mononuclear cells, as shown in Fig. 2B (d and h). In addition, a PLA experiment was performed using MR16-1 as a primary antibody on the damaged muscle cross sections at day 3 (Fig. S1). The distributions of PLA signals were similar to those shown in Fig. 2B d and h. These results indicated that MR16-1 was located in the damaged muscle.

3.4. MR16-1 levels in the damaged muscle

Changes of MR16-1 levels in the damaged muscle during the course of regeneration were investigated by western blot analysis. Both HC and LC levels declined significantly from day 3 to 7 after injury with CTX (Fig. 3A and B). We also investigated whether the decrease of MR16-1 levels was related to the short half-life of MR16-1 or to a reduction of its target, IL-6R. The first possibility was examined by analyzing the responses of HC and LC levels to 2 bouts of MR16-1 administration immediately and 3 days after induction of injury. However, the levels of both HC and LC at day 7 were identical between the muscles receiving 1 bout and those receiving 2 bouts of MR16-1 treatment (Fig. 3B).

To test the second possibility, the expressions of IL-6R and gp130 were analyzed at days 3 and 7 post-injury by real-time PCR (Fig. 3C and D). Both IL-6R and gp130 expressions were significantly up-regulated 3 days after CTX injury and down-regulated thereafter. The changes in the IL-6R expression during muscle regeneration normalized by 18S were almost identical to the data normalized by GAPDH (data not shown). Furthermore, the protein level of IL-6R in the damaged muscles was also significantly greater than in the control at day 3, but was down-regulated at day 7 (Fig. 3E and F), and these findings were perfectly matched with the shift of mRNA levels. Taken together, these results indicated that the decrease in the level of MR16-1 from day 3 to 7 may have been closely related to a reduction of IL-6R level.

3.5. IL-6R expression in infiltrated mononucleated cells

Since MR16-1 was detected in the necrotic fibers and infiltrated mononuclear cells, this localization may have been modulated by the amount of IL-6R expression. Therefore, we next investigated the cause of the elevation of IL-6R level. PLA signals for IL-6R were mainly detected in the area with infiltrated mononucleated cells (Fig. 4a–d), supporting the localization of MR16-1 shown in Fig. 2B d and h. In addition, PLA signals for IL-6R were weakly observed around the necrotic fibers (Fig. 4e–h).

CD68, which is one of the markers for macrophages, was predominantly detected in the area where the mononuclear cells were accumulated (Fig. 5a and c). Similar staining patterns were noted in response to CD11b antibody, which marks both macrophages and neutrophils, in the same area of the serial cross section (Fig. S3A a and c). However, the staining of the serial muscle cross sections did not show any immunoreactivity for the neutrophil marker in the same area (Fig. 5d and f). In the interstitial areas of the muscle cross section at day 1 post-injury,

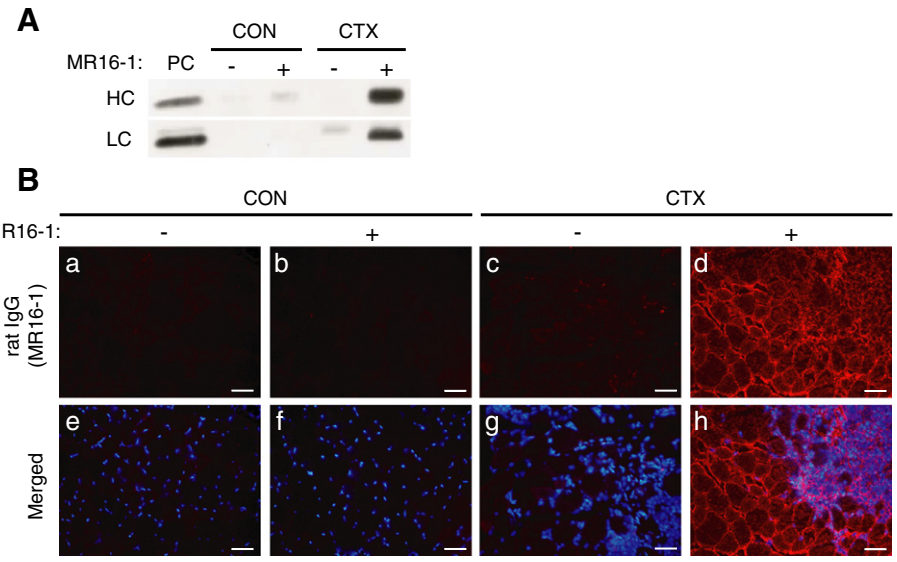

Fig. 2. Specific delivery of rat anti-mouse interleukin-6 receptor antibody (MR16-1) to the damaged region of muscle. A: Western blot analyses in undamaged (CON) and damaged (with cardiotoxin, CTX) muscles with (+) or without (−) MR16-1 treatment. Western blots show both heavy chain (HC, 50 kDa) and light chain (LC, 25 kDa). As a positive control (PC), MR16-1 itself was loaded. B: Proximity ligation assay analyses in CON and CTX muscles. Scale bar = 50 μm.

however, positive stainings for the neutrophil marker and CD11b were observed (Fig. S3B a, c, d and f). In contrast, CD68-positive cells were hardly detectable at day 1 post-injury (Fig. S3B g and i). In addition, double staining of CD68 and IL-6R was conducted, and revealed the co-localization of CD68 and IL-6R at 3 days post-injury (Fig. 5g–l). These results suggested that the robust increase of IL-6R expression following CTX injury was mainly derived from infiltration of CD68-positive macrophages.

3.6. Phosphorylation of STAT3 during muscle inflammation

It has previously been considered that IL-6 signaling is potentially transduced via the activation of Janus kinases and the recruitment and phosphorylation of STAT family members such as STAT3. Therefore, the levels of total STAT3 and phosphorylation of STAT3 (pSTAT3) of muscle extracts at days 3 and 7 after CTX injury were examined by western blot analysis. The bands of pSTAT3 were not detected in non-damaged muscle at any time points, irrespective of whether the treatment with MR16-1 was applied (Fig. 6A). Increased expression of STAT3 and elevation of the pSTAT3 level were seen at days 3 and 7 following injury. The total STAT3 protein levels remained constantly high throughout the experimental period. However, the pSTAT3 level appeared to decrease with time. The phosphorylation of STAT3 in damaged muscle was significantly inhibited by treatment with MR16-1 at day 3 post-injury (Fig. 6A and B). However, a significant inhibitory effect of MR16-1 administration on the level of pSTAT3 was not seen at day 7 post-injury.

PLA signals for pSTAT3 were detected in the macrophage-enriched area and in necrotic fibers (Fig. 6C and D). However, the number of PLA signals in the macrophage-enriched area was significantly higher

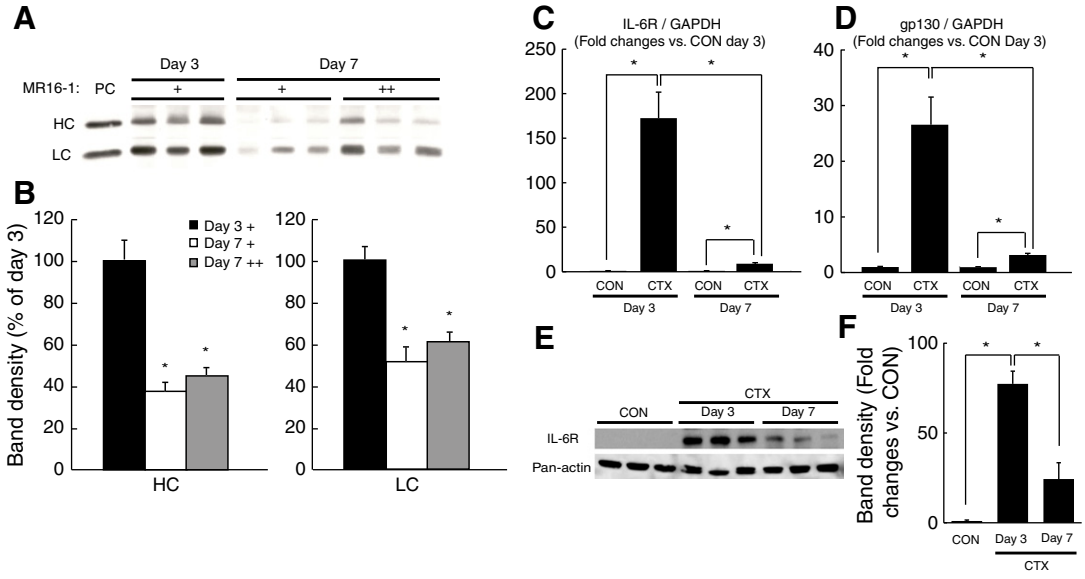

Fig. 3. Time-course changes of MR16-1 levels remaining in the damaged muscle. A: The levels of MR16-1, which was injected i.p. once (+) or twice (++) immediately and 3 days after induction of injury. B: Densities of HC and LC bands. Values are the means ± SEM. n = 6/group. *: $p < 0.05$ vs. day 3. Data were expressed as a percentage vs. the level at day 3 (100%). C and D: Time-course changes of the mRNA expression of interleukin-6 receptor (IL-6R) and gp130 in muscles with (CTX) and without injuries (CON). GAPDH: glyceraldehyde 3-phosphate dehydrogenase. Values are the means ± SEM. n = 4/group. E: Changes of IL-6R expression in damaged muscles by western blot analysis. F: Densities of IL-6R bands. Values are the means ± SEM. n = 3/group. *: $p < 0.05$ vs. CON. See Fig. 2 for other abbreviations.

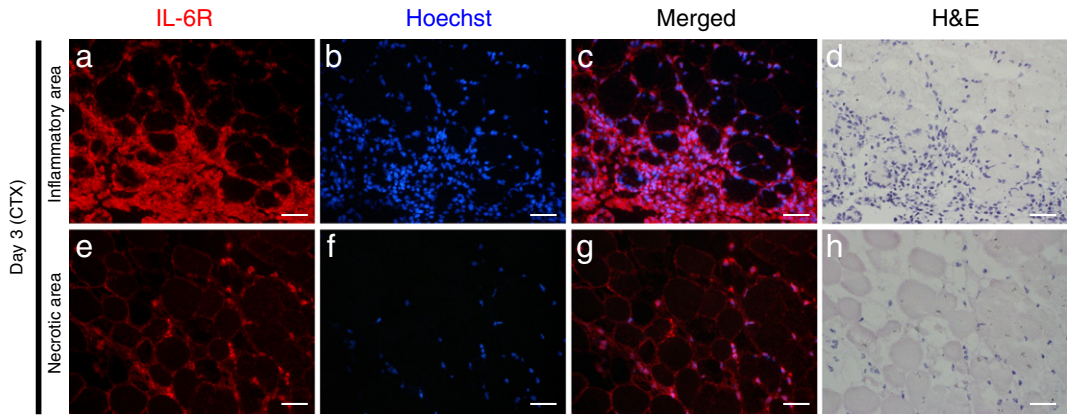

Fig. 4. Expression of IL-6R in the inflammatory and necrotic areas of muscle cross sections 3 days after injection of CTX. Prominent IL-6R signals (red) were detected (a, c, e, and g). The cross sections were re-stained with hematoxylin and eosin (H&E) (d and h). All of these stainings were performed in the same areas of samples. Scale bar = 50 μm. See Figs. 2 and 3 for other abbreviations.

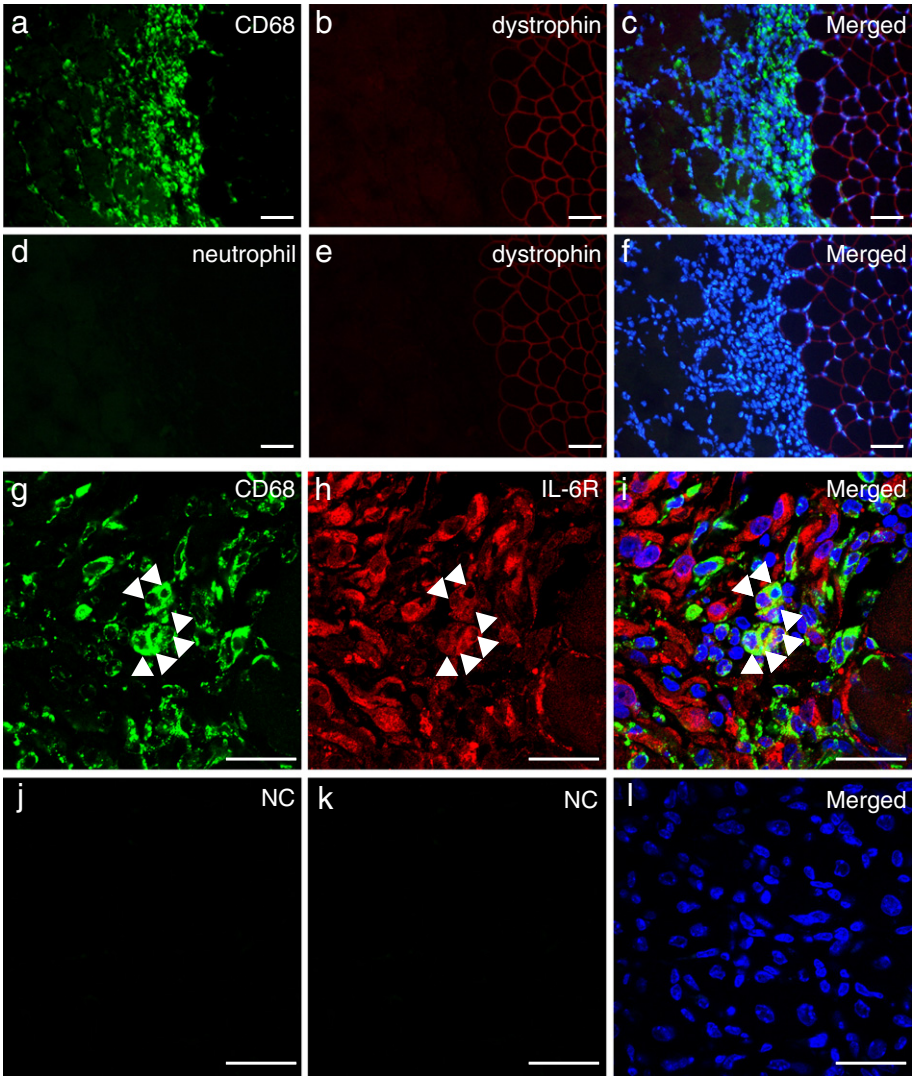

Fig. 5. Immunohistochemical evaluation of IL-6R on infiltrated mononuclear cells at day 3 post-injury. Cells stained positively with CD68 (green), neutrophil, dystrophin (red) and nuclei (blue) are shown (a–f). Staining with dystrophin (red) was used to detect necrotic lesions (dystrophin negative; left side of b and e). The intact area, which was not injured by CTX injection, was dystrophin-positive (right side of b and e). The results of co-staining with CD68 (green) and IL-6R (red) are shown (g–i). Arrowheads indicate the co-localization of CD68 and IL-6R. Staining for the negative control (NC) without any primary antibodies (j–l). Scale bar = 50 μm. See Fig. 2 for other abbreviations.

than that in the area of necrotic fibers (CTX: 926 ± 99 in the macrophage-enriched area vs. 374 ± 43 in the area of necrosis, $p < 0.01$; CTX + MR16-1: 510 ± 107 vs. 217 ± 49 in the same areas, $p < 0.05$). Importantly, the number of PLA signals was significantly lower in the macrophage-enriched area of the MR16-1-treated mice than in that of the untreated mice (Fig. 6E). The number of PLA signals in the section stained without the primary antibody (background signal) was 88.3 ± 18.7 (n = 3).

The levels of total STAT3 and pSTAT3 of muscle extracts at days 3 and 7 after CTX injury in IL-6$^{-/-}$ mice were also examined. The phosphorylation of STAT3 in damaged muscle was significantly inhibited in IL-6$^{-/-}$ mice, compared with wild type (WT) mice, at day 3 post-injury (Fig. 6F and G). At day 7 after injury, there was no significant difference in pSTAT3 levels between IL-6$^{-/-}$ and WT mice (Fig. 6F and G).

3.7. Immunohistochemical analyses for muscle regeneration

Relative to the well-arranged myofibers with peripheral nuclei in the normal control muscles (Fig. 7A a and b), some swollen myofibers lightly stained by eosin and with many inflammatory cells were observed in the damaged muscles at day 3 (Fig. 7A c and e). Inflammatory cells still remained at day 7, although their distribution was drastically reduced from day 3 (Fig. 7A d and f). Further, newly regenerating myofibers with central nuclei were also observed.

To examine whether MR16-1 treatment stimulated muscle regeneration, the number of myogenin^{+} cells (arrows in Fig. 7B a–i) was quantified, and the results indicated that MR16-1 treatment significantly increased the number of myogenin^{+} cells compared with that in non-treated damaged muscle (Fig. 7C). The number of myogenin^{+}/desmin^{+}

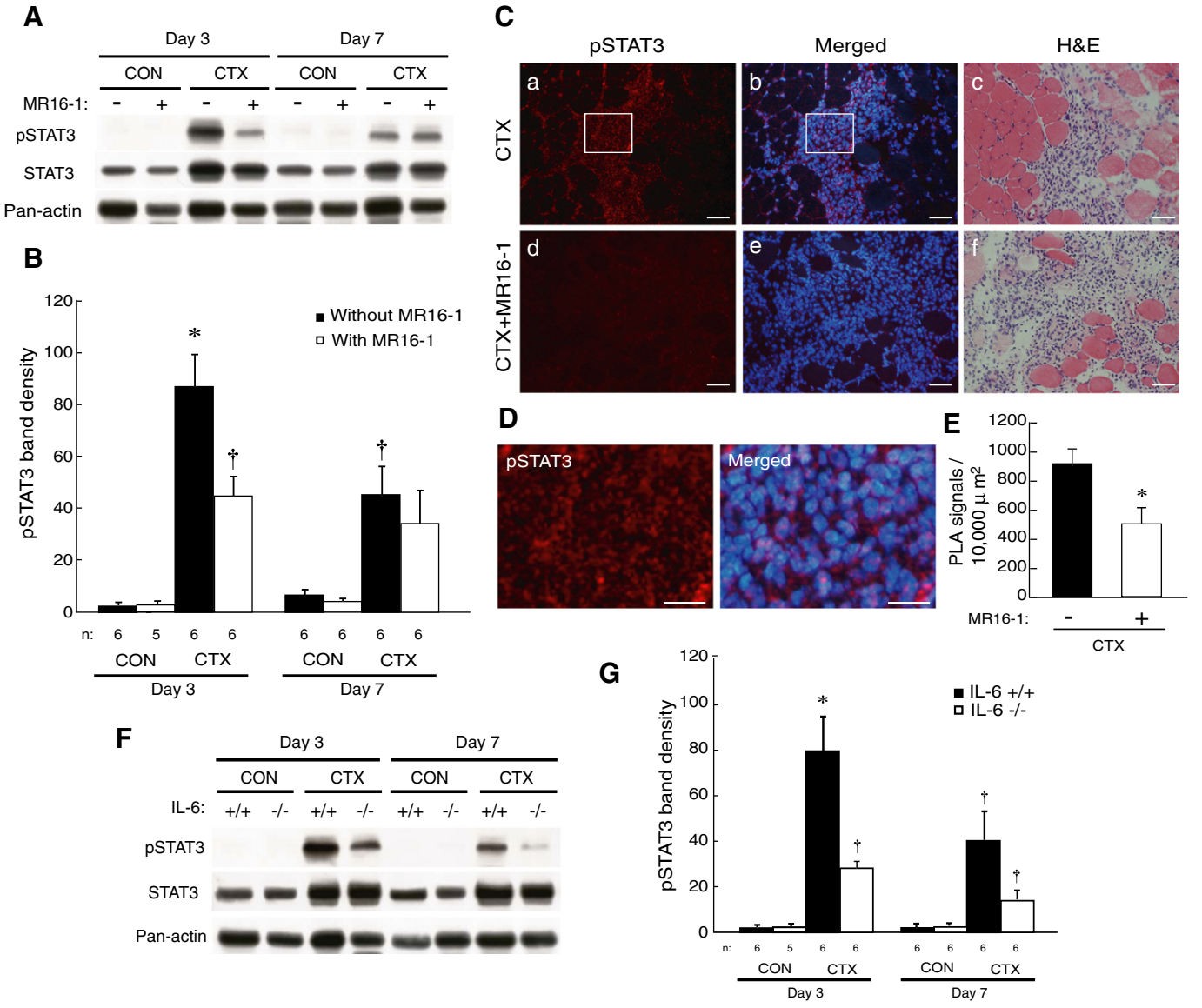

Fig. 6. Effects of the blockade of phosphorylation of signal transducer and activator of transcription 3 (STAT3) by MR16-1 treatment. A: Western blot analyses of phosphorylated STAT3 (pSTAT3), STAT3, and Pan-actin (loading control) in undamaged (CON) and damaged (CTX) muscles with (+) or without (−) MR16-1 treatment were performed 3 and 7 days after injury. B: Quantified band densities of pSTAT3/STAT3 in A. n = 5–6/group. Values are the means ± SEM. *: $p < 0.05$ vs. CON and CON + MR16-1; †: $p < 0.05$ vs. CTX at day 3 without MR16-1. C: Proximity ligation assay (PLA) analyses for pSTAT3 (red), nuclei (blue), and H&E in the damaged muscle cross sections at day 3 post-injury with (CTX + MR16-1) or without MR16-1 treatment (CTX). a–c and d–f: identical areas, respectively. D: Enlarged images of the areas in the white squares in C a and b. The scale bars in C and D are 50 μm and 20 μm, respectively. E: Total number of PLA signals in the area with infiltrated macrophages. Values are the means ± SEM. n = 5/group. *: $p < 0.05$. F: Western blot analyses of pSTAT3, STAT3, and Pan-actin (loading control) in undamaged (CON) and damaged muscles with injection of CTX of both wild type (+/+) and IL-6 knock-out (−/−) mice. G: Quantified band densities of pSTAT3/STAT3 in E. n = 5–6/group. *: $p < 0.05$ vs. CON (+/+) and CON (−/−) at day 3; †: $p < 0.05$ vs. CTX (+/+) at day 3. See Figs. 2 and 4 for other abbreviations.

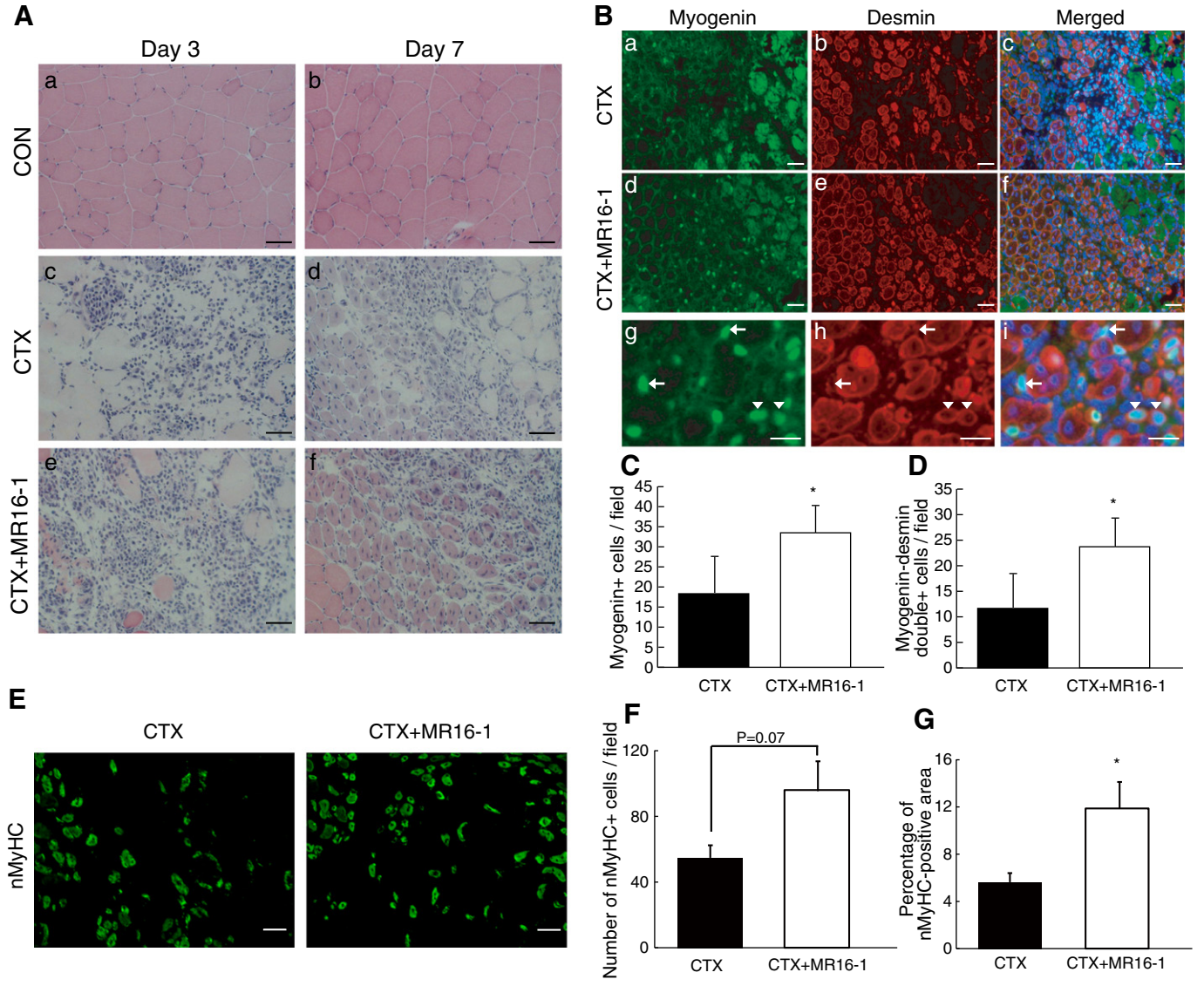

Fig. 7. Histological evaluation of muscle regeneration. A: Representative muscle sections stained by H&E at days 3 and 7 post-injury with or without MR16-1 treatment. B: Immunohistochemically stained images of myogenin (green) and desmin (red) in damaged muscle at day 7 post-injury. g–i: Enlarged images of the myogenin positive ($^+$, arrow) and myogenin and desmin double$^+$ cells (arrowheads). Nuclei were stained with 4′,6-diamidino-2-phenylindole (DAPI, blue). C and D: Number of myogenin$^+$ and myogenin and desmin double$^+$ cells, respectively. Values are the means ± SEM. n = 6/group. *: $p < 0.05$. Scale bars = 50 μm (A: a–f; B: a–f) and 20 μm (B: g–i). E: Immunohistochemical analyses of neonatal myosin heavy chain (nMyHC) expressions in damaged muscle at day 7 post-injury. F: Number of nMyHC$^+$ cells in muscle cross-sections. G: Percentage area of nMyHC$^+$ cells in muscle cross-sections. Values are the means ± SEM. n = 3–4/group. *: $p < 0.05$. Scale bars = 50 μm. See Figs. 2 and 4 for other abbreviations.

cells, indicated by the arrowheads in the enlarged images in Fig. 7B g–i, was also significantly increased in the damaged muscle treated with MR16-1 compared with the non-treated damaged muscle (Fig. 7D). In addition, neonatal myosin heavy chain (nMyHC)$^+$ cells were assessed in regenerating muscles with or without MR16-1 treatment (Fig. 7E, F and G). The nMyHC expression was generally detected in newly formed myotubes, but not in mature myofibers. The number of nMyHC$^+$ cells tended to be increased by MR16-1 treatment, but not to a statistically significant degree (Fig. 7F, $p = 0.07$). However, the percentage area of MyHC$^+$ cells in regenerating muscle subjected to MR16-1 treatment was significantly higher than that in non-treated damaged muscle (Fig. 7G). These data suggested that MR16-1 accelerated the muscle regeneration after CTX-induced injury.

3.8. Gene expressions in the LMD-isolated macrophage-enriched area

Since MR16-1 treatment affected the CD68-positive macrophages expressing IL-6R in the present study, we hypothesized that the modulated gene expression in those cells played a role in the acceleration of myogenesis by MR16-1 treatment. To investigate the responses of the gene expressions in macrophages, the macrophage-enriched (CD68-positive) areas were isolated by LMD 3 days after CTX injury with or without MR16-1 treatment in WT mice and IL-6$^{-/-}$ mice (Fig. 8A). Real-time PCR showed that the expressions of TNF-α and IL-1β, the major pro-inflammatory cytokines, were decreased in the macrophage-enriched areas following MR16-1 treatment, although these differences did not reach the statistically significant level (Fig. 8B a and b). The expression of iNOS was not influenced by treatment with MR16-1 (Fig. 8B c). The expressions of IL-10 and arginase, which were associated with tissue fibrosis, were significantly decreased by MR16-1 treatment (Fig. 8B d and e). In addition, the increased expressions of IL-10 and arginase were also inhibited in IL-6$^{-/-}$ mice, which was similar to the results observed in response to MR16-1 treatment (Fig. 8B d and e). However, the TNF-α and IL-1β levels in IL-6$^{-/-}$ mice were not different from those detected in WT mice with MR16-1 treatment (Fig. 8B a and b). The expression of iNOS was also not influenced by the deletion of IL-6 (Fig. 8B c).

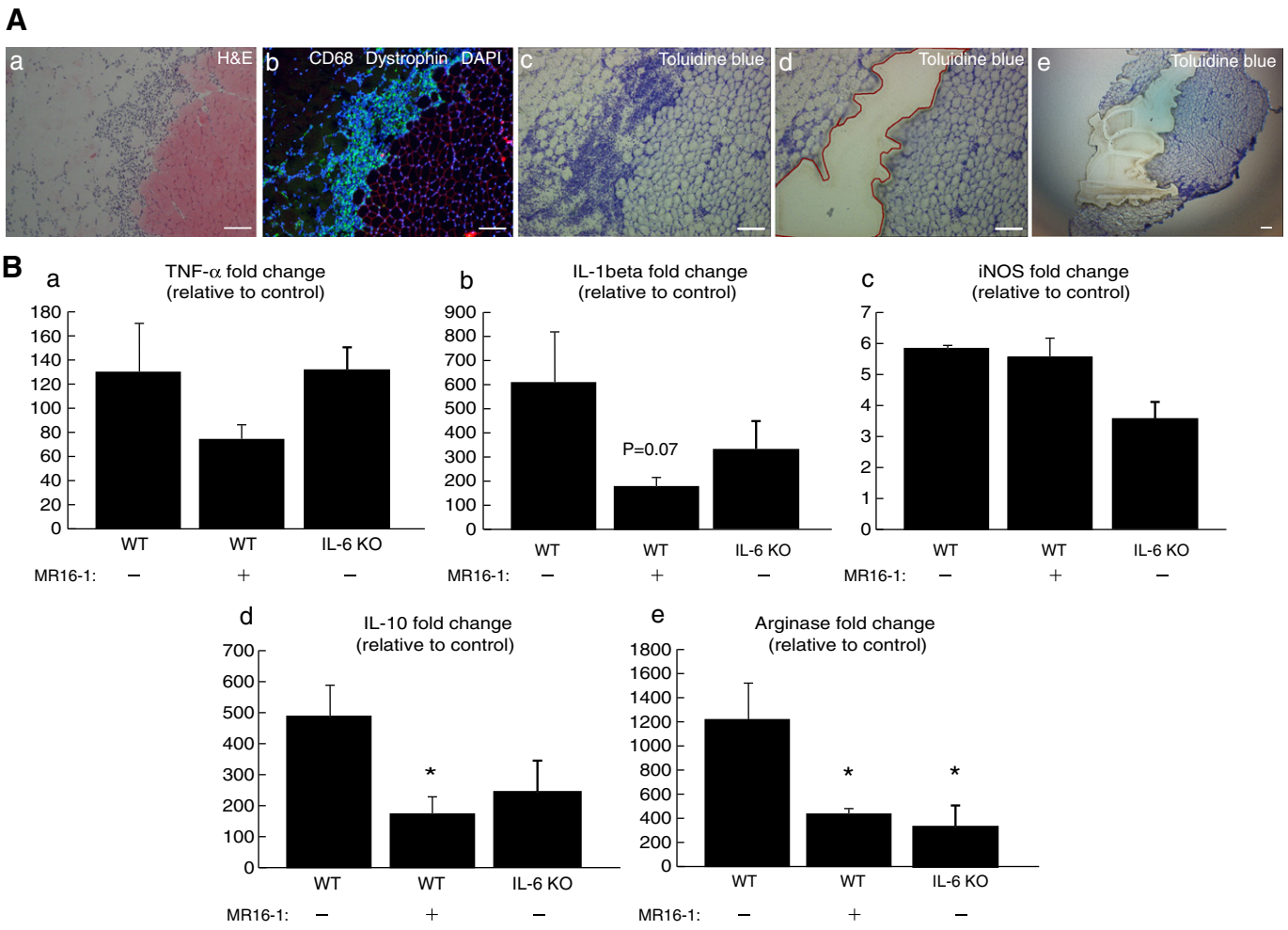

Fig. 8. Effects of MR16-1 treatment on the gene expression in macrophage-enriched areas. A: Serial cross sections of damaged muscles at day 3 post-injury stained with H&E (a), anti-CD68 (green), and anti-dystrophin (red) antibodies, and with DAPI (blue) (b) and toluidine blue (c–e) are shown. A whole view of the muscle section after laser capture microdissection (LMD) is shown in e. The area marked with a red line was isolated (c, d). All scale bars in panel a–e = 100 μm. B: Effect of MR16-1 treatment and IL-6 deletion on gene expression in LMD-isolated macrophage-enriched areas: a, tumor necrosis factor-α (TNF-α); b, interleukin-1β (IL-1β); c, inducible nitric oxide synthase (iNOS); d, interleukin-10 (IL-10); and e, arginase. Values are the means ± SEM. n = 4/group. *: $p < 0.05$ vs. WT without MR16-1 treatment. See Figs. 2, 4, and 7 for other abbreviations.

4. Discussion

Three major results were noted. First, the administered anti-mouse IL-6R antibody, MR16-1, was delivered to the CTX-induced damaged muscles. This delivery was positively correlated with the IL-6R expression levels. Secondly, treatment with MR16-1 resulted in reduced phosphorylation of STAT3 in the macrophage-enriched area, where IL-6R was highly expressed at day 3 after CTX injury. Finally, MR16-1 treatment after CTX-induced damage accelerated the skeletal muscle regeneration, in association with an increased number of myogenin$^+$/desmin$^+$ cells and increased nMyHC-positive myotube area.

Currently, cytokines are used for the treatment of a variety of pathological conditions, including RA, polymyositis, and/or Duchenne muscular dystrophy [26,30,36]. However, the mechanism by which these agents are delivered to the damaged tissue is not clear yet. Wakabayashi et al. [37] tried to visualize MR16-1 by using biotinylated MR16-1, but the distribution of MR16-1 within the damaged region could be determined. Here, by using western blotting and PLA, we demonstrated that the i.p.-administered MR16-1 was present in the damaged muscle, but not in the contralateral undamaged muscle. Thus, MR16-1 was suggested to play an important role in the treatment of damaged tissues. Moreover, the results depicted in Fig. 3 indicated that the time-course-dependent reduction of the MR16-1 level in the damaged muscle was attributable to a drastic reduction in the IL-6R expression level from day 3 to 7 after injury. A phenomenon similar to the change in IL-6R expression after injury was also seen for the pSTAT3 level, which was elevated at day 3 post-injury and decreased at day 7. However, whether i.p.-injected MR16-1 was specifically delivered to damaged muscles was still not clear, because the extra-cellular matrix in injured tissues was usually sticky and cross-reacted with non-specific proteins. Therefore, further studies will be needed to determine whether or not MR16-1 is specifically distributed to damaged muscle.

In the CTX-induced muscle injury model, the expression of IL-6 in damaged muscle increased markedly at day 3 post-injury, and this up-regulation was constantly maintained up to day 7 post-injury (Fig. S4A). Although the IL-6 protein levels were markedly increased in damaged muscles at day 3, this up-regulation had dropped sharply at day 7 post-injury (Fig. S4B). These data suggest that IL-6/IL-6R signaling might play a large role in the early phase of muscle regeneration (inflammatory phase). IL-6 signaling is mediated by the activation of Janus kinase and the recruitment and phosphorylation of STAT family members such as STAT3. A significant inhibitory effect of MR16-1 on phosphorylation of STAT3 was found at day 3 post-injury, but not at day 7 post-injury, possibly due to insufficient expression of IL-6/IL-6R signaling. The possibility that the injected MR16-1 might have been degraded within 7 days was rejected, since the levels of MR16-1 were identical in response to single- and double-injection treatment. Takagi and colleagues [33] reported that, when MR16-1 was administered to

patients with late-phase collagen-induced arthritis, it appeared to have no inhibitory effect on the disease development, even though the production of IL-6 was detected. These results lead us to conclude that we should focus on not only the IL-6 expression level, but also the IL-6R expression level, in order to improve the performance of MR16-1 treatment under some pathological conditions.

MR16-1 treatment did not affect the macrophage recruitment in the present study. However, it was reported previously that MR16-1 treatment after spinal cord injury reduced the inflammatory cell accumulation [29,31]. One of the possible causes for these disparate results might be that TNF-α and IL-1β, which play critical roles for the infiltration of macrophages into injured tissue, were not significantly changed by MR16-1 treatment.

The acceleration of muscle regeneration by MR16-1 treatment was confirmed by the increases in myogenin$^+$, myogenin$^+$/desmin$^+$ cells and newly formed myotubes with nMyHC. This positive effect of MR16-1 on muscle regeneration may have been ascribable to the reduced level of macrophage-induced IL-10 and arginase expressions. It is also known that Th2 cytokines, such as IL-10, can activate M2 macrophages, and this activation may drive muscle fibrosis through arginine metabolism by arginase [38]. Therefore, it was suggested that the administration of MR16-1 suppressed the secretion of fibrosis-related cytokines derived from macrophages. The subsequent enhancement of myogenesis might be triggered by the inhibited fibrosis, which could interfere with the muscle regeneration.

In addition to Th2 cytokines, it has been reported that IL-1β promotes fibroblast formation through the activation of transforming growth factor-β (TGF-β) [5,39]. Although no significant influence of MR16-1 treatment on IL-1β was observed in the present study, its expression tended to decrease following the treatment with MR16-1 (Fig. 8B b). Marked decreases of IL-10 and arginase in infiltrated macrophages by MR16-1 treatment were noted, but other fibrosis-related genes, including IL-13 and TGF-β, were not measured in the present study. Hence, further studies considering a larger number of fibrosis-related genes in macrophages are required to reveal the precise mechanism responsible for the prevention of fibrosis by treatment with MR16-1.

There is no direct evidence that down-regulations of IL-10 and arginase are affected by a reduction of pSTAT3 in infiltrated macrophages. Phosphorylation of STAT3 was also inhibited at day 3 after injury in IL-6 null mice, compared with wild type mice (Fig. 6F and G). In addition, the overall tendency in the changes of gene expression in the LMD-isolated macrophage-enriched areas of muscle in IL-6 null mice was similar to those observed in response to MR16-1 treatment (Fig. 8B d and e), except in the cases of TNF-α and IL-1β (Fig. 8B a and b). The different responses of TNF-α and IL-1β may have been related to the up-regulation of these pro-inflammatory cytokines in IL-6 null mice by compensatory mechanisms. It has been reported that MR16-1 treatment suppresses the activity of matrix metalloprotease-2 (MMP-2), which plays a critical role in the development of fibrogenesis, after myocardial infarction [31,40], and reduces scar tissue formation after spinal cord injury [31,40]. Activation of STAT3 is known to promote MMP-2 expression through interaction with the MMP-2 promoter [41]. Therefore, these data suggest that MR16-1 suppresses the phosphorylation of STAT3 and the subsequent modulation of fibrosis-related genes, such as IL-10 and arginase.

The prevention and amelioration of fibrosis are clinically important for the efficient regeneration of muscle from severe damage, because the development of fibrosis after injury is known to hinder muscle regeneration and to prevent the recovery to full strength [5,6]. In the present study, it was suggested that the inhibition of IL-6 signaling may prevent fibrosis and promote rapid myogenesis after CTX-induced injury, even though it has also been reported that IL-6 facilitates muscle growth via the activation of satellite cells [21,34]. This disparity might be partly explained by the finding that MyoD$^+$ satellite cells are present only at very low numbers at day 3 after CTX-induced muscle injury [42]. Thus, since prominent IL-6R expression in infiltrated CD68$^+$ macrophages is noted at day 3 post-injury, the direct effects of MR16-1 on the activation of satellite cells are not particularly significant. This possibility was also supported by a previous study demonstrating that IL-6R and gp130 mRNA expressions were not observed in newly formed myogenin-expressing myotubes after contusion [43]. Taking these findings together, we consider that the acceleration of myogenesis by MR16-1 treatment seen in the present study might have been mainly achieved by the modulation of fibrosis-related genes in inflammatory macrophages.

Moreover, the results of the present study provide clinically relevant evidence that the subsequent reduction of IL-6R in damaged tissue may reflect a need for IL-6 signaling, which may be a good predictor of the effectiveness of MR16-1 treatment for several types of diseases and conditions.

In conclusion, the present study demonstrated that MR16-1 treatment reduces gene expressions associated with fibrogenesis in infiltrated macrophages, and thus MR16-1 might facilitate muscle regeneration via immune modulation. Therefore, the effectiveness of IL-6-signal blockade by MR16-1 should be a focus on another muscle disease models such as mdx mouse (DMD mouse model), in which virtually skeletal muscle function is compromised by fibrosis.

Supplementary data to this article can be found online at http://dx.doi.org/10.1016/j.bbagen.2014.01.014.

Acknowledgements

This study was supported by Grant-in-Aid for Scientific Research (S, 19100009 to Y.O.; C, 20500577 to N.N.) and Grant-in-Aid for JSPS Fellows (12J03873 to R.F.) from the Japan Society for the Promotion of Science and Grants-in-Aid for Young Scientists B (19700521 and 21700656 to F.K.) from the Ministry of Education, Culture, Sports, Science and Technology, Japan.

References

[1] S.B. Charge, M.A. Rudnicki, Cellular and molecular regulation of muscle regeneration, Physiol. Rev. 84 (2004) 209–238.
[2] S. Ciciliot, S. Schiaffino, Regeneration of mammalian skeletal muscle. Basic mechanisms and clinical implications, Curr. Pharm. Des. 16 (2010) 906–914.
[3] J.G. Tidball, Inflammatory processes in muscle injury and repair, Am. J. Physiol. Regul. Integr. Comp. Physiol. 288 (2005) R345–R353.
[4] J.G. Tidball, S.A. Villalta, Regulatory interactions between muscle and the immune system during muscle regeneration, Am. J. Physiol. Regul. Integr. Comp. Physiol. 298 (2010) R1173–R1187.
[5] L. Pelosi, C. Giacinti, C. Nardis, G. Borsellino, E. Rizzuto, C. Nicoletti, F. Wannenes, L. Battistini, N. Rosenthal, M. Molinaro, A. Musaro, Local expression of IGF-1 accelerates muscle regeneration by rapidly modulating inflammatory cytokines and chemokines, FASEB J. 21 (2007) 1393–1402.
[6] K. Sato, Y. Li, W. Foster, K. Fukushima, N. Badlani, N. Adachi, A. Usas, F.H. Fu, J. Huard, Improvement of muscle healing through enhancement of muscle regeneration and prevention of fibrosis, Muscle Nerve 28 (2003) 365–372.
[7] M. Segawa, S. Fukada, Y. Yamamoto, H. Yahagi, M. Kanematsu, M. Sato, T. Ito, A. Uezumi, S. Hayashi, Y. Miyagoe-Suzuki, S. Takeda, K. Tsujikawa, H. Yamamoto, Suppression of macrophage functions impairs skeletal muscle regeneration with severe fibrosis, Exp. Cell Res. 314 (2008) 3232–3244.
[8] N. Dumont, P. Bouchard, J. Frenette, Neutrophil-induced skeletal muscle damage: a calculated and controlled response following hindlimb unloading and reloading, Am. J. Physiol. Regul. Integr. Comp. Physiol. 295 (2008) R1831–R1838.
[9] L. Arnold, A. Henry, F. Poron, Y. Baba-Amer, N. van Rooijen, A. Plonquet, R.K. Gherardi, B. Chazaud, Inflammatory monocytes recruited after skeletal muscle injury switch into antiinflammatory macrophages to support myogenesis, J. Exp. Med. 204 (2007) 1057–1069.
[10] N. Dumont, J. Frenette, Macrophages protect against muscle atrophy and promote muscle recovery in vivo and in vitro: a mechanism partly dependent on the insulin-like growth factor-1 signaling molecule, Am. J. Pathol. 176 (2010) 2228–2235.
[11] J.G. Tidball, M. Wehling-Henricks, Macrophages promote muscle membrane repair and muscle fibre growth and regeneration during modified muscle loading in mice in vivo, J. Physiol. 578 (2007) 327–336.
[12] S.A. Villalta, H.X. Nguyen, B. Deng, T. Gotoh, J.G. Tidball, Shifts in macrophage phenotypes and macrophage competition for arginine metabolism affect the severity of muscle pathology in muscular dystrophy, Hum. Mol. Genet. 18 (2009) 482–496.
[13] S. Gordon, F.O. Martinez, Alternative activation of macrophages: mechanism and functions, Immunity 32 (2010) 593–604.

[14] S. Gordon, P.R. Taylor, Monocyte and macrophage heterogeneity, Nat. Rev. Immunol. 5 (2005) 953–964.
[15] R.D. Stout, C. Jiang, B. Matta, I. Tietzel, S.K. Watkins, J. Suttles, Macrophages sequentially change their functional phenotype in response to changes in microenvironmental influences, J. Immunol. 175 (2005) 342–349.
[16] D. Ruffell, F. Mourkioti, A. Gambardella, P. Kirstetter, R.G. Lopez, N. Rosenthal, C. Nerlov, A CREB-C/EBPbeta cascade induces M2 macrophage-specific gene expression and promotes muscle injury repair, Proc. Natl. Acad. Sci. U. S. A. 106 (2009) 17475–17480.
[17] S.E. Chen, E. Gerken, Y. Zhang, M. Zhan, R.K. Mohan, A.S. Li, M.B. Reid, Y.P. Li, Role of TNF-{alpha} signaling in regeneration of cardiotoxin-injured muscle, Am. J. Physiol. Cell Physiol. 289 (2005) C1179–C1187.
[18] S.E. Chen, B. Jin, Y.P. Li, TNF-alpha regulates myogenesis and muscle regeneration by activating p38 MAPK, Am. J. Physiol. Cell Physiol. 292 (2007) C1660–C1671.
[19] M. Cheng, M.H. Nguyen, G. Fantuzzi, T.J. Koh, Endogenous interferon-gamma is required for efficient skeletal muscle regeneration, Am. J. Physiol. Cell Physiol. 294 (2008) C1183–C1191.
[20] F. Haddad, F. Zaldivar, D.M. Cooper, G.R. Adams, IL-6-induced skeletal muscle atrophy, J. Appl. Physiol. 98 (2005) 911–917.
[21] A.L. Serrano, B. Baeza-Raja, E. Perdiguero, M. Jardi, P. Munoz-Canoves, Interleukin-6 is an essential regulator of satellite cell-mediated skeletal muscle hypertrophy, Cell Metab. 7 (2008) 33–44.
[22] T. Tsujinaka, J. Fujita, C. Ebisui, M. Yano, E. Kominami, K. Suzuki, K. Tanaka, A. Katsume, Y. Ohsugi, H. Shiozaki, M. Monden, Interleukin 6 receptor antibody inhibits muscle atrophy and modulates proteolytic systems in interleukin 6 transgenic mice, J. Clin. Invest. 97 (1996) 244–249.
[23] T. Tsujinaka, M. Kishibuchi, M. Yano, T. Morimoto, C. Ebisui, J. Fujita, A. Ogawa, H. Shiozaki, E. Kominami, M. Monden, Involvement of interleukin-6 in activation of lysosomal cathepsin and atrophy of muscle fibers induced by intramuscular injection of turpentine oil in mice, J. Biochem. 122 (1997) 595–600.
[24] S. Acharyya, S.M. Sharma, A.S. Cheng, K.J. Ladner, W. He, W. Kline, H. Wang, M.C. Ostrowski, T.H. Huang, D.C. Guttridge, TNF inhibits Notch-1 in skeletal muscle cells by Ezh2 and DNA methylation mediated repression: implications in Duchenne muscular dystrophy, PLoS One 5 (2010).
[25] M.D. Grounds, H.G. Radley, B.L. Gebski, M.A. Bogoyevitch, T. Shavlakadze, Implications of cross-talk between tumour necrosis factor and insulin-like growth factor-1 signalling in skeletal muscle, Clin. Exp. Pharmacol. Physiol. 35 (2008) 846–851.
[26] M.D. Grounds, J. Torrisi, Anti-TNFalpha (Remicade) therapy protects dystrophic skeletal muscle from necrosis, FASEB J. 18 (2004) 676–682.
[27] T. Kishimoto, T. Taga, S. Akira, Cytokine signal transduction, Cell 76 (1994) 253–262.
[28] N. Nishimoto, T. Kishimoto, Inhibition of IL-6 for the treatment of inflammatory diseases, Curr. Opin. Pharmacol. 4 (2004) 386–391.
[29] M. Mukaino, M. Nakamura, O. Yamada, S. Okada, S. Morikawa, F. Renault-Mihara, A. Iwanami, T. Ikegami, Y. Ohsugi, O. Tsuji, H. Katoh, Y. Matsuzaki, Y. Toyama, M. Liu, H. Okano, Anti-IL-6-receptor antibody promotes repair of spinal cord injury by inducing microglia-dominant inflammation, Exp. Neurol. 224 (2010) 403–414.
[30] N. Nishimoto, K. Yoshizaki, N. Miyasaka, K. Yamamoto, S. Kawai, T. Takeuchi, J. Hashimoto, J. Azuma, T. Kishimoto, Treatment of rheumatoid arthritis with humanized anti-interleukin-6 receptor antibody: a multicenter, double-blind, placebo-controlled trial, Arthritis Rheum. 50 (2004) 1761–1769.
[31] S. Okada, M. Nakamura, Y. Mikami, T. Shimazaki, M. Mihara, Y. Ohsugi, Y. Iwamoto, K. Yoshizaki, T. Kishimoto, Y. Toyama, H. Okano, Blockade of interleukin-6 receptor suppresses reactive astrogliosis and ameliorates functional recovery in experimental spinal cord injury, J. Neurosci. Res. 76 (2004) 265–276.
[32] M. Okazaki, Y. Yamada, N. Nishimoto, K. Yoshizaki, M. Mihara, Characterization of anti-mouse interleukin-6 receptor antibody, Immunol. Lett. 84 (2002) 231–240.
[33] N. Takagi, M. Mihara, Y. Moriya, N. Nishimoto, K. Yoshizaki, T. Kishimoto, Y. Takeda, Y. Ohsugi, Blockage of interleukin-6 receptor ameliorates joint disease in murine collagen-induced arthritis, Arthritis Rheum. 41 (1998) 2117–2121.
[34] B.R. McKay, M. De Lisio, A.P. Johnston, C.E. O'Reilly, S.M. Phillips, M.A. Tarnopolsky, G. Parise, Association of interleukin-6 signalling with the muscle stem cell response following muscle-lengthening contractions in humans, PLoS One 4 (2009) e6027.
[35] K. Kami, E. Senba, In vivo activation of STAT3 signaling in satellite cells and myofibers in regenerating rat skeletal muscles, J. Histochem. Cytochem. 50 (2002) 1579–1589.
[36] N. Okiyama, T. Sugihara, Y. Iwakura, H. Yokozeki, N. Miyasaka, H. Kohsaka, Therapeutic effects of interleukin-6 blockade in a murine model of polymyositis that does not require interleukin-17A, Arthritis Rheum. 60 (2009) 2505–2512.
[37] K. Wakabayashi, M. Fujioka, S. Kanzaki, H.J. Okano, S. Shibata, D. Yamashita, M. Masuda, M. Mihara, Y. Ohsugi, K. Ogawa, H. Okano, Blockade of interleukin-6 signaling suppressed cochlear inflammatory response and improved hearing impairment in noise-damaged mice cochlea, Neurosci. Res. 66 (2010) 345–352.
[38] M. Wehling-Henricks, M.C. Jordan, T. Gotoh, W.W. Grody, K.P. Roos, J.G. Tidball, Arginine metabolism by macrophages promotes cardiac and muscle fibrosis in mdx muscular dystrophy, PLoS One 5 (2010) e10763.
[39] B. Vidal, A.L. Serrano, M. Tjwa, M. Suelves, E. Ardite, R. De Mori, B. Baeza-Raja, M. Martinez de Lagran, P. Lafuste, V. Ruiz-Bonilla, M. Jardi, R. Gherardi, C. Christov, M. Dierssen, P. Carmeliet, J.L. Degen, M. Dewerchin, P. Munoz-Canoves, Fibrinogen drives dystrophic muscle fibrosis via a TGFbeta/alternative macrophage activation pathway, Genes Dev. 22 (2008) 1747–1752.
[40] M. Kobara, K. Noda, M. Kitamura, A. Okamoto, T. Shiraishi, H. Toba, H. Matsubara, T. Nakata, Antibody against interleukin-6 receptor attenuates left ventricular remodelling after myocardial infarction in mice, Cardiovasc. Res. 87 (2010) 424–430.
[41] T.X. Xie, D. Wei, M. Liu, A.C. Gao, F. Ali-Osman, R. Sawaya, S. Huang, Stat3 activation regulates the expression of matrix metalloproteinase-2 and tumor invasion and metastasis, Oncogene 23 (2004) 3550–3560.
[42] D. Sun, C.O. Martinez, O. Ochoa, L. Ruiz-Willhite, J.R. Bonilla, V.E. Centonze, L.L. Waite, J.E. Michalek, L.M. McManus, P.K. Shireman, Bone marrow-derived cell regulation of skeletal muscle regeneration, FASEB J. 23 (2009) 382–395.
[43] K. Kami, Y. Morikawa, M. Sekimoto, E. Senba, Gene expression of receptors for IL-6, LIF, and CNTF in regenerating skeletal muscles, J. Histochem. Cytochem. 48 (2000) 1203–1213.